CTCV J2056-3014: An X-Ray-faint Intermediate Polar Harboring an Extremely Fast-spinning White Dwarf

R. Lopes de Oliveira[1,2] [ORCID], A. Bruch[3], C. V. Rodrigues[4] [ORCID], A. S. Oliveira[5] [ORCID], and K. Mukai[6,7] [ORCID]

[1] Departamento de Física, Universidade Federal de Sergipe, Av. Marechal Rondon, S/N, 49000-000 São Cristóvão, SE, Brazil; rlofilho@academico.ufs.br
[2] Observatório Nacional, Rua Gal. José Cristino 77, 20921-400, Rio de Janeiro, RJ, Brazil
[3] Laboratório Nacional de Astrofísica, Rua Estados Unidos, 154, CEP 37504-364, Itajubá, MG, Brazil
[4] Divisão de Astrofísica, Instituto Nacional de Pesquisas Espaciais, 12227-010, São José dos Campos, SP, Brazil
[5] IP&D, Universidade do Vale do Paraíba, 12244-000, São José dos Campos, SP, Brazil
[6] CRESST II and X-ray Astrophysics Laboratory, NASA Goddard Space Flight Center, Greenbelt, MD 20771, USA
[7] Center for Space Science and Technology, University of Maryland, Baltimore County, 1000 Hilltop Circle, Baltimore, MD 21250, USA
Received 2020 July 8; revised 2020 July 13; accepted 2020 July 14; published 2020 July 30

Abstract

We report on XMM-Newton X-ray observations that reveal CTCV J2056-3014 to be an unusual accretion-powered, intermediate polar (IP) system. It is a member of the class of X-ray-faint IPs whose space density remains unconstrained but potentially very high, with $L_{x,0.3-12\,keV}$ of 1.8×10^{31} erg s^{-1}. We discovered a coherent 29.6 s pulsation in X-rays that was also revealed in our reanalysis of published optical data, showing that the system harbors the fastest-spinning, securely known white dwarf (WD) so far. There is no substantial X-ray absorption in the system. Accretion occurs at a modest rate ($\sim 6 \times 10^{-12}\,M_\odot$ yr^{-1}) in a tall shock above the WD, while the star seems to be spinning in equilibrium and to have low magnetic fields. Further studies of CTCV J2056-3014 potentially have broad implications on the origin of magnetic fields in WDs, on the population and evolution of magnetic cataclysmic variables, and also on the physics of matter around rapidly rotating magnetic WDs.

Unified Astronomy Thesaurus concepts: Cataclysmic variable stars (203); X-ray binary stars (1811); DQ Herculis stars (407)

1. Introduction

CTCV J2056-3014 (hereafter J2056) is a cataclysmic variable (CV) with an orbital period of 1.76 hr determined from time-resolved optical spectroscopy (Augusteijn et al. 2010). Based on their detection of a short periodicity at 15.4 min from optical photometry and the fact that the system matches a relatively bright X-ray emitter in the ROSAT (PSPC) Bright Source Catalog (0.10 ± 0.02 cts s^{-1} at 0.1–2.4 keV; Haakonsen & Rutledge 2009), Augusteijn et al. (2010) suggested J2056 to be an intermediate polar (IP) candidate, i.e., an asynchronously rotating magnetic white dwarf (WD) accreting matter from a Roche-lobe-filling donor usually via a partial accretion disk (Patterson 1994).

Oliveira et al. (2017) presented additional optical spectroscopy of the system and pointed out the similarity of its spectrum to the spectral features found in the rare IPs with short orbital periods. These features include Hβ as intense as Hα and weak He II 4686 Å in emission. Optical photometry of J2056 conducted by Bruch (2018) revealed that the averaged magnitude of the system varies by at least 2.4 mag in comparison with measurements of Augusteijn et al. (2010), ranging from $V \sim 17.6$ to 15.2 mag, and that it displays strong flickering with an amplitude up to 0.8 mag. Bruch (2018) also suggested that the 15.4 min period claimed by Augusteijn et al. (2010) is spurious. Finally, Gaia parallax indicates that J2056 is a nearby system, at a distance (d) of 261.6 ± 7.4 pc (Bailer-Jones et al. 2018).

We have started an XMM-Newton X-ray follow-up program for validation of CV candidates originally identified in optical surveys, which includes J2056. Here we report on its X-ray properties, which suggest J2056 to be an unusual IP. We also revisit the optical observations of Bruch (2018).

2. Observations

2.1. X-Ray Data

J2056 was observed for about 18 ks on 2019 October 24 by XMM-Newton (ObsID 0842570101; PI: R. Lopes de Oliveira). The snapshot was focused on X-ray spectrophotometry with the European Photon Imaging Camera (EPIC), namely MOS1, MOS2, and pn cameras. The Reflection Grating Spectrometers RGS1 and RGS2 did not collect enough photons to allow us to carry out high-resolution X-ray spectroscopy. The UV observations with the Optical Monitor in timing mode barely covered the source position, rendering its data unusable for timing analysis.

The EPIC observations were partially contaminated by solar particles, with only a low background level during about 15.2 ks for the MOS cameras, and 8.7 ks for the pn camera. No pile-up or technical issues were identified in these data. The observations were reduced and data products were extracted following standard procedures using the Science Analysis System (SAS) v18.0.0. In particular, they were reprocessed using the EPPROC (for the pn data) and EMPROC (for the MOS1-2 data) tasks. We used calibration files downloaded on 2020 January 2. Spectral analysis was accomplished using the XSPEC software version 12.9.1 m.

2.2. Optical Data

We revisited the optical photometric observations of J2056 presented by Bruch (2018) with the sole purpose of checking for high-frequency periodicities. This effort was motivated by the detection of pulsation in X-rays (Section 3.2). The optical observations were carried out on four nights in 2015 (June 9–12) and on two nights in 2016 (September 7–8) with the 0.6 m Zeiss telescope of Observatório do Pico dos Dias—
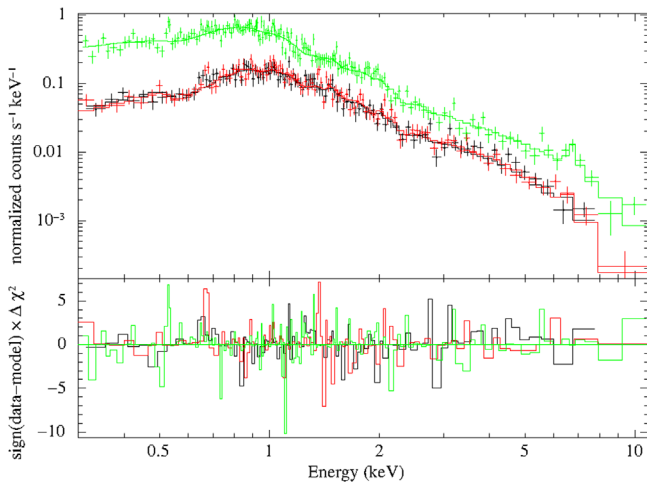
Figure 1. X-ray spectra (top) and residuals (bottom): black, red, and green colors correspond to MOS1, MOS2, and pn data, respectively. The continuous lines are the single thermal plus cooling-flow emission model fits to the data.

Laboratório Nacional de Astrofísica, Brazil. Light curves spanning from 55 to 340 min were obtained with a time resolution of 5 s. To maximize the count rates within the short exposures, no filter was used. The throughput of the instrumentation corresponded roughly to V magnitude (Bruch 2018). Basic data reduction (bias removal, flat-fielding) and aperture photometry were performed using default procedures with IRAF (Tody 1986) and with the MIRA (Bruch 1993) software system, respectively.

3. Results

3.1. X-Ray Spectroscopy

The net count rates of J2056 at 0.3–12 keV were 0.194 ± 0.004 counts s^{-1}, 0.202 ± 0.004 counts s^{-1}, and 0.739 ± 0.010 counts s^{-1} for the MOS1, MOS2, and pn cameras, respectively. The spectra were binned such that each bin had at least 25 counts and thus the χ^2 method was applied to both fit and test statistics in their modeling with XSPEC.

Even with relatively short exposures, the observations resulted in good-quality EPIC spectra (Figure 1). The X-ray energy distribution of J2056 extends over the whole energy range covered by the EPIC cameras. An excess emission due to ionized lines of the Fe Kα complex at 6.6–7 keV is seen in the pn data and supports the interpretation, usual in accreting WDs, of the predominantly thermal nature for the X-ray emission. There is no evidence of an optically thick, blackbody-like component from the WD surface. Thus, we applied the following XSPEC models that account for the emission from collisionally ionized diffuse gas due to accretion as the primary energy source: APEC, describing a single thermal plasma, and MKCFLOW, a multi-temperature model representing a cooling flow (Mushotzky & Szymkowiak 1988). The MKCFLOW model was interpolated using the AtomDB (Foster et al. 2012) data so that it is equivalent in assumptions to those used in the APEC model. We adopted the abundance table of Asplund et al. (2009). The PHABS model was used to account for the photoelectric absorption effects on X-rays.

A single temperature component (PHABS*APEC) does not match the spectra well, failing to explain the continuum below 2 keV and the Fe Kα complex ($\chi^2_\nu = 2.18$). The inclusion of a second thermal component (PHABS*(APEC+APEC)) improves

the fit but fails especially in the description of the 0.9–1.5 keV region and slightly overpredicts the Fe Kα lines ($\chi^2_\nu = 1.19$). Despite similar statistics ($\chi^2_\nu = 1.18$), the cooling flow model (PHABS*MKCFLOW) visually improves the description of both continuum and iron lines. Finally, an acceptable description ($\chi^2_\nu = 1.09$) is found by adding a single thermal component to the cooling-flow model, providing a good fit of the 1 keV region, which is expected to be rich in unresolved emission lines. As for the MKCFLOW, we fixed the unconstrained kT_{low} parameter to its minimum value of 0.0808 keV and the required redshift parameter to 6.1×10^{-8} from the Gaia distance and standard cosmological values of XSPEC. Table 1 lists the best-fit spectral parameters of the models described above. Figure 1 shows the EPIC spectra and the final model PHABS*(APEC +MKCFLOW); henceforth, this is the model discussed in this Letter.

Our best-fit model indicates that the X-rays are absorbed by the equivalent in hydrogen column density (N_{H}) of $2.7^{+0.7}_{-0.7} \times 10^{20}$ cm^{-2}. The X-ray emission is dominated by a moderately hard thermal component that cools down from $kT = 14.34^{+1.18}_{-1.21}$ keV. A secondary contribution is well described by a plasma component having $kT = 0.79^{+0.04}_{-0.04}$ keV, which accounts for about 6.2% of the total unabsorbed flux at 0.3–12 keV. A subsolar abundance of $0.81^{+0.16}_{-0.14}$ $Z_\odot$ is inferred, forced to be the same for both thermal components during the fits, but its determination strongly depends on the Fe Kα lines. From the MKCFLOW component, the mass accretion rate is $5.9^{+0.5}_{-0.4} \times 10^{-12}$ $M_\odot$ yr^{-1}. The total luminosity of the system at 0.3–12 keV is $1.8 \times 10^{31}(d/261.6 \text{ pc})^2$ erg s^{-1}. These results are discussed in Section 4.

3.2. X-Ray and Optical Timing Analysis

Time flags were converted to the Barycentric Dynamical Timescale using the online tool[8] of Eastman et al. (2010) for the optical observations and the BARYCEN/SAS task for the X-ray data. Background-corrected X-ray light curves from each EPIC camera were produced considering a binning of 10 s. We considered three energy ranges: 0.3–10 keV, 0.3–2 keV ("soft"), and 2–10 keV ("hard"), in order to access the energy dependence of any variable signal. The light curves of each EPIC camera were investigated separately. Optical light curves were constructed retaining the original resolution of 5 s.

The search for periodicities was carried out using the Lomb–Scargle periodogram (Lomb 1976; Scargle 1982) in optical and X-ray light curves. We explored X-ray light curves considering two data sets. The first incorporates the entire observations. It includes spikes in background count rates, which can be as high as the source signal, especially in the 2–10 keV band. This condition lasted for about 2.6 ks. The second considers only data that were collected during the last ~7.5 ks, the longest continuous time interval with low particle background.

A high-significance peak associated with a period of 29.6 s is clearly seen in the Lomb–Scargle periodogram applied to the 0.3–10 and 0.3–2 keV light curves of all EPIC cameras (Figure 2). As for the 2–10 keV band, the peak is recovered only in light curves produced considering a time interval with low background contamination, and with a lower power when compared to results of the other two energy ranges. This is

---

8 See http://astroutils.astronomy.ohio-state.edu/time.

Table 1
Best-fit Spectral X-Ray Parameters

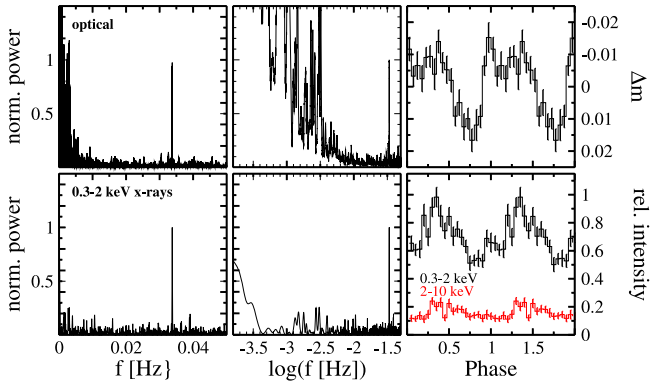|	N_H $(10^{20}$ cm$^{-2})$	kT_{apec} (keV)	kT_{apec} (keV)	$kT_{max,mkcflow}$ (keV)	Z $(\times Z_\odot)$	χ^2_ν/d.o.f.	Unabs. flux$_{(0.3-12\ keV)}$ (erg cm^{-2} s^{-1})	$L_{0.3-12keV}$ (erg s^{-1})
PHABS*(APEC+APEC)	$2.4^{+0.6}_{-0.6}$	$0.81^{+0.02}_{-0.02}$	$5.11^{+0.24}_{-0.24}$	...	$0.74^{+0.14}_{-0.13}$	1.19/386	2.1×10^{-12}	$1.7 \times 10^{31}(d/261.6$ pc$)^2$ erg s^{-1}
PHABS*MKCFLOW	$2.9^{+0.5}_{-0.5}$	...	...	$9.88^{+0.35}_{-0.39}$	$0.80^{+0.10}_{-0.09}$	1.18/388	2.1×10^{-12}	$1.7 \times 10^{31}(d/261.6$ pc$)^2$ erg s^{-1}
PHABS*(APEC +MKCFLOW)	$2.7^{+0.7}_{-0.7}$	$0.79^{+0.04}_{-0.04}$	...	$14.34^{+1.18}_{-1.21}$	$0.81^{+0.16}_{-0.14}$	1.09/386	2.2×10^{-12}	$1.8 \times 10^{31}(d/261.6$ pc$)^2$ erg s^{-1}

Figure 2. Periodograms and folded light curves on the 29.6 s period from the optical (top) and X-ray (bottom; from pn) data. For X-rays, the periodograms corresponding to the soft band and light curves are shown for the soft and hard bands.

mainly due to the low signal-to-noise ratio in the hard energy range.

As reported by Bruch (2018), the optical light curve of J2056 displays variations on timescales of hours superposed by flickering. A search for high-frequency periodicities in optical data was first carried out individually for each of the six nights. The 29.6 s pulsation seen in X-rays is also identified in all optical light curves, and the periods in both regions are the same at the level of the formal errors. The upper left and center panels of Figure 2 show the periodogram of the 2015 June 10 optical light curve. The optical data taken in subsequent nights do not indicate migration of phase. We refine the periodicity in the optical by merging the light curves of each of the two observing seasons, resulting in an average period of 29.6098 ± 0.0014 s.[9] The same value was derived from the 0.3–2 keV pn light curve considering the entire observation, but with an uncertainty of ± 0.0213 s.

Figure 2 (right frames) shows folded optical and X-ray light curves. Before folding the optical data on the 29.6 s period, variations on longer timescales were removed from the light curve by subtraction of a filtered version generated by the Savitzky–Golay algorithm (Savitzky & Golay 1964) which eliminates variations below a cutoff timescale, here chosen to be 1 min. We adopted a conservative approach and used the free-flare data set to construct the phase-folded, X-ray light curves. It still covers ∼250 pulsation cycles and avoids features that may be background-induced.

The waveform in the optical phase diagram is characterized by a deep minimum and two maxima of approximately equal height, separated by about 0.4 in phase (see the upper right

frame of Figure 2). The semi-amplitude of these variations is ∼0.016 mag, and its shape is quite similar to that observed in soft X-rays (0.3–2 keV), except for the difference in height of the X-ray maxima. The pulsed fraction is significant in all light curves. In the soft band, the variability reaches about 25% of the mean level. A similar value is obtained for the integrated band because the total counts are dominated (∼80%) by soft X-ray photons. As for "hard" (2–10 keV) X-rays, even though the pulsation is not as clearly observed in the periodograms, the folded light curve indicates that the 29.6 s modulation is present and has a significant (∼50%) pulsed fraction (see Figure 2).

Optical and X-ray modulations can be understood within the same scenario. The stability of the 29.6 s modulation over two years in the optical (2015 and 2016) and its presence three years later in X-rays (2019) lead us to the interpretation that it represents the spin period of the WD in J2056.

4. Discussions and Conclusions

Our main findings are: (i) J2056 is an IP harboring a fast-spinning WD, and (ii) its X-ray luminosity is low for an IP. Those properties together with the short orbital period (1.76 hr; Augusteijn et al. 2010), below the CV orbital period gap and rare among IPs, make J2056 an unusual and interesting IP.

Many IPs have been discovered through INTEGRAL and Swift/BAT hard X-ray ($E > 10$ keV) surveys (de Martino et al. 2020), for which interstellar absorption is not an issue. They have typically L_X above 10^{33} erg s^{-1} meaning that, with the available sensitivities, the systems can be discovered out beyond 1 kpc (Pretorius & Mukai 2014). Although large enough to yield a statistically significant sample of luminous IPs, the hard X-ray source catalogs are small enough (<2000 objects) for systematic identification and follow-up programs (see, e.g., Halpern et al. 2018; de Martino et al. 2020). However, there appears to be a separate class of low-luminosity IPs (LLIPs; Pretorius & Mukai 2014) typically with L_X ∼10^{31} erg s^{-1}, only a subset of which have been detected in hard X-ray all-sky surveys (Mukai 2017). The LLIP population seems to be dominated by short orbital period systems (Pretorius & Mukai 2014), but there is no known unique set of characteristics that allows us to readily identify its members to construct a distance-limited, complete sample. As argued by Pretorius & Mukai (2014), the separate and yet not constrained LLIP population may be numerous enough to match the common IPs in integrated X-ray luminosity. Thus, many LLIPs may be awaiting discovery. In this context, the identification of J2056 as an LLIP is significant.

J2056 has the fastest-spinning WD among confirmed IPs and also holds the record of all securely known WDs. We are aware of only two systems that may be harboring a WD rotating faster than J2056: WZ Sge and RX J0648.0-4418. WZ Sge exhibits

---

[9] Note that the time difference between the two seasons is too large to concatenate the two data sets without cycle count ambiguities and thus to refine the period even more.

intermittent modulations at 27.87 and 28.96 s, which may be associated with the rotation of its WD, but this identification is not secure (see the results and discussion in Nucita et al. 2014). RX J0648.0-4418 contains a 1.28 $M_\odot$ (Mereghetti et al. 2009) compact object spinning at 13.2 s (Israel et al. 1997) but its nature is not clear: it may be a WD in an early evolutionary stage (Popov et al. 2018) or a neutron star. Mereghetti et al. (2016) argued that the spin-up rate derived for RX J0648.0-4418 (2.15×10^{-15} s s^{-1}) would be unusual for an accreting WD and this scenario would be strongly disfavoured if the distance is confirmed to be less than $\sim$4 kpc. And, in fact, the system seems to be much nearer: $d_{\mathrm{Gaia}} = 501.1^{+16.7}_{-15.6}$ pc (Bailer-Jones et al. 2018). Moreover, we notice that the bulk of the X-ray emission is interpreted as being due to a non-thermal (power-law) component (Mereghetti et al. 2013), which is not expected for an accreting WD but is the rule for accreting neutron stars

Two lines of argument strongly suggest that the magnetic field of J2056 is low for an IP. The first is to assume that J2056, as is likely for IPs as a group (Patterson et al. 1919), is in spin equilibrium. Consideration of material torques (which act to spin up the WD) and magnetic torques (which must balance the material torques in equilibrium) leads to the conclusion that the magnetic fields of fast-spinning IPs, such as J2056, are lower than their longer spin period cousins (see Equation (21) and Figure 17 of Patterson 1994). This assumption leads to a preliminary estimate of magnetic moment $\mu \sim 5 \times 10^{30}$ G cm^3 for J2056 but this needs to be revisited after further studies. Note that this is not a conclusion that applies to all LLIPs, because at least two systems have relatively long spin periods —EX Hya with 4021.6 s (e.g., Mauche et al. 2009) and V1025 Cen with 2146.59 s (Buckley et al. 1998). The second argument, instead of the spin equilibrium assumption, relies on the fact that accretion is suppressed when the inner edge of the disk is rotating more slowly than the magnetic field lines. Such systems are believed to behave as magnetic propellers (see the case of AE Aqr; Wynn et al. 1997). Since J2056 is entirely consistent with being accretion-powered and does not display any signatures of a propeller, the Keplerian frequency at the inner edge of its disk must be $\sim$29.6 s or shorter. Such a small magnetospheric radius, combined with the modest accretion rate (Section 3.1), demands a low magnetic field.

The X-ray emission can be explained by the cooling flow framework expected for accretion-powered WDs, plus a single thermal plasma that responds for about 6% of the total luminosity (Section 3.1). The latter contribution likely represents a marked deviation from the assumptions behind the MKCFLOW model, which are expected to be violated in the condition of a tall shock along which the accreting matter is expected to suffer non-negligible gravitational acceleration. In fact, the luminosity and therefore the accretion rate per unit area, is low, suggesting that the shock is not occurring near the WD surface. Under these conditions, the often-made assumptions of radial accretion, freefall from infinity, and shock near the WD surface are not applicable and thus the maximum temperature of the shock (in this case $kT = 14.34^{+1.18}_{-1.21}$ keV) cannot be directly used to determine the mass of the WD (which under such assumptions would be around 0.46 $M_\odot$).

The tridimensional extinction map of Lallement et al. (2019) combined with a Gaia distance of 260 pc suggest a best-guess $E(B-V)$ of 0.014 mag that corresponds to $N_{\mathrm{H}} \sim 1.2 \times 10^{20}$ cm^{-2}, but one as high as 0.033 mag indicating $N_{\mathrm{H}} \sim 2.5 \times 10^{20}$ cm^{-2} in the line of sight to J2056 is still possible. The value inferred from X-rays (Section 3.1) is $N_{\mathrm{H}} = 2.9^{+0.5}_{-0.5} \times 10^{20}$ cm^{-2}, which is at most only slightly higher than that due to the interstellar medium. Thus, contrary to what is typical in luminous IPs, there is no significant intrinsic X-ray absorption in J2056.

The lack of a strong intrinsic (complex) absorber for J2056 is another common characteristic of LLIPs (see, for example, the case of DW Cnc; Nucita et al. 2019). The low absorption in J2056 is an additional piece of evidence for a tall shock. This is because tall shocks allow us to see the X-rays from the side of the post-shock region with no expectation of being affected by a complex absorber. The opposite is a common characteristic of classic (luminous) IPs, in which the shock is near the WD surface and our lines of sight almost inevitably cross a strong complex absorber in the pre-shock flow.

J2056 is entirely accretion-powered, which is an important finding if compared with other objects with similar spin periods. AE Aqr, a peculiar IP harboring a WD with a spin period of 33 s (and orbital period of 9.88 hr) and with an even lower X-ray luminosity than J2056, is thought to be in the propeller regime (Welsh et al. 1998). AR Sco has a WD with a spin period of 117 s (orbital period of 3.56 hr) and may even be entirely rotation-powered, as a "white-dwarf pulsar" (Marsh et al. 2016; Buckley et al. 2017).

The example of J2056, displaying X-rays that are not luminous or hard enough to have attracted attention in previous surveys, leads to a promising strategy to identify further LLIPs by follow-up X-ray observations of short orbital period CVs and candidates. The eROSITA survey will likely reveal the true extent of the LLIP population by measuring the X-ray fluxes of all known CVs and discovering many new ones (Schwope & eROSITA Collaboration 2019). This is important for advancing our understanding of the physics and evolutionary history of these systems. In fact, J2056, with its low X-ray luminosity and the fast spin of its WD, may be typical of a currently unrecognized sub-population of the class. If that is the case, implying that there is a large population of lower magnetic field IPs, this is an important clue that must be factored into the theory of the origin of the magnetic field in WDs, and that of the population and evolution of magnetic CVs. Moreover, J2056 offers an important test case for the physics of matter around a rapidly rotating magnetic WD.

Facilities: XMM-Newton(EPIC/MOS1, EPIC/MOS2, and EPIC/pn), LNA:0.6-m Zeiss.

Software: XSPEC (Arnaud 1996), SAS (https://cosmos.esa.int/), IRAF (Tody 1986), MIRA (Bruch 1993).

ORCID iDs

R. Lopes de Oliveira ⓘ https://orcid.org/0000-0002-6211-7226
C. V. Rodrigues ⓘ https://orcid.org/0000-0002-9459-043X
A. S. Oliveira ⓘ https://orcid.org/0000-0001-6422-9486
K. Mukai ⓘ https://orcid.org/0000-0002-8286-8094

References

Arnaud, K. A. 1996, in ASP Conf. Ser. 101, Astronomical Data Analysis Software and Systems V, ed. G. H. Jacoby & J. Barnes (San Francisco, CA: ASP), 17
Asplund, M., Grevesse, N., Sauval, A. J., & Scott, P. 2009, ARA&A, 47, 481

Augusteijn, T., Tappert, C., Dall, T., & Maza, J. 2010, MNRAS, 405, 621
Bailer-Jones, C. A. L., Rybizki, J., Fouesneau, M., Mantelet, G., & Andrae, R. 2018, AJ, 156, 58
Bruch, A. 1993, MIRA: A Reference Guide (Münster: Univ. Münster)
Bruch, A. 2018, NewA, 58, 53
Buckley, D. A. H., Cropper, M., Ramsay, G., & Wickramasinghe, D. T. 1998, MNRAS, 299, 83
Buckley, D. A. H., Meintjes, P. J., Potter, S. B., Marsh, T. R., & Gänsicke, B. T. 2017, NatAs, 1, 0029
de Martino, D., Bernardini, F., Mukai, K., Falanga, M., & Masetti, N. 2020, AdSpR, 66, 1209
Eastman, J., Siverd, R., & Gaudi, B. S. 2010, PASP, 122, 935
Foster, A. R., Ji, L., Smith, R. K., & Brickhouse, N. S. 2012, ApJ, 756, 128
Haakonsen, C. B., & Rutledge, R. E. 2009, ApJS, 184, 138
Halpern, J. P., Thorstensen, J. R., Cho, P., et al. 2018, AJ, 155, 247
Israel, G. L., Stella, L., Angelini, L., et al. 1997, ApJL, 474, L53
Lallement, R., Babusiaux, C., Vergely, J. L., et al. 2019, A&A, 625, A135
Lomb, N. R. 1976, Ap&SS, 39, 447
Marsh, T. R., Gänsicke, B. T., Hümmerich, S., et al. 2016, Natur, 537, 374
Mauche, C. W., Brickhouse, N. S., Hoogerwerf, R., et al. 2009, IBVS, 5876, 1
Mereghetti, S., la Palombara, N., Tiengo, A., et al. 2013, A&A, 553, A46
Mereghetti, S., Pintore, F., Esposito, P., et al. 2016, MNRAS, 458, 3523
Mereghetti, S., Tiengo, A., Esposito, P., et al. 2009, Sci, 325, 1222
Mukai, K. 2017, PASP, 129, 062001
Mushotzky, R. F., & Szymkowiak, A. E. 1988, in Cooling Flows in Clusters and Galaxies, NATO Advanced Science Institutes (ASI) Series C, Vol. 229, ed. A. C. Fabian (Dordrecht: Kluwer), 53
Nucita, A. A., Conversi, L., & Licchelli, D. 2019, MNRAS, 484, 3119
Nucita, A. A., Kuulkers, E., de Paolis, F., et al. 2014, A&A, 566, A121
Oliveira, A. S., Rodrigues, C. V., Cieslinski, D., et al. 2017, AJ, 153, 144
Patterson, J. 1994, PASP, 106, 209
Patterson, J., de Miguel, E., Kemp, J., et al. 1919, ApJ, 897, 70
Popov, S. B., Mereghetti, S., Blinnikov, S. I., Kuranov, A. G., & Yungelson, L. R. 2018, MNRAS, 474, 2750
Pretorius, M. L., & Mukai, K. 2014, MNRAS, 442, 2580
Savitzky, A., & Golay, M. J. E. 1964, AnaCh, 36, 1627
Scargle, J. D. 1982, ApJ, 263, 835
Schwope, A. & eROSITA Collaboration 2019, in Compact White Dwarf Binaries, ed. G. H. Tovmassian & B. T. Gansicke, 49
Tody, D. 1986, Proc. SPIE, 627, 733
Welsh, W. F., Horne, K., & Gomer, R. 1998, MNRAS, 298, 285
Wynn, G. A., King, A. R., & Horne, K. 1997, MNRAS, 286, 436